

Biophysical Journal, Volume 121

Supplemental information

Elastic versus brittle mechanical responses predicted for dimeric cadherin complexes

Brandon L. Neel, Collin R. Nisler, Sanket Walujkar, Raul Araya-Secchi, and Marcos Sotomayor

SUPPORTING MATERIAL

Elastic versus Brittle Mechanical Responses Predicted for Dimeric Cadherin Complexes

Running Title: Simulated Elasticity of Cadherin Dimers

Brandon L. Neel^{1,2†}, Collin R. Nisler^{1,3†}, Sanket Walujkar^{1,4†}, Raul Araya-Secchi⁵, and Marcos Sotomayor^{1,2,3,4*}

¹ Department of Chemistry and Biochemistry, The Ohio State University
484 W 12th Avenue, Columbus, OH 43210, USA

² The Ohio State Biochemistry Program, The Ohio State University
484 W 12th Avenue, Columbus, OH 43210, USA

³ Biophysics Graduate Program, The Ohio State University
484 W 12th Avenue, Columbus, OH 43210, USA

⁴ Chemical Physics Graduate Program, The Ohio State University
484 W 12th Avenue, Columbus, OH 43210, USA

⁵ Facultad de Ingeniería y Tecnología, Universidad San Sebastián,
Santiago, Chile

† Co-first authors.

* Corresponding author - Marcos Sotomayor, sotomayor.8@osu.edu

2022

ORCIDs

Brandon L. Neel: 0000-0001-5983-9335

Collin R. Nisler: 0000-0002-3054-0556

Sanket Walujkar: 0000-0002-5892-4578

Raul Araya-Secchi: 0000-0002-4872-3553

Marcos Sotomayor: 0000-0002-3333-1805

Supplementary Discussion

Dissociation constants measured in equilibrium indicate that the mouse CDH1 homophilic bond is weak ($K_D \sim 96.5 \pm 10.6 \mu\text{M}$ at 25°C for EC1-2 and $K_D \sim 109 \pm 6 \mu\text{M}$ for EC1-5 from analytical ultracentrifugation [AUC] experiments) (1, 2) while heterophilic binding between full-length ectodomains of human DSG2 and DSC1 is stronger ($K_D \sim 11.52 \pm 0.2 \mu\text{M}$ at 25°C from plasmon resonance [SPR] experiments) (3), and the homophilic interactions for DSG2 and DSC1 are not detected in SPR or bead aggregation experiments, despite bond formation in crystal structures, presumably suggesting weaker binding as indicated by AUC experiments ($K_D \sim 433 \pm 102 \mu\text{M}$ and $K_D \sim 39 \pm 0 \mu\text{M}$, respectively, at 25°C) (3) and atomic force microscopy (AFM) experiments ($K_D \sim 412 \mu\text{M}$ with unbinding force peaks between 20 pN and 40 pN) (4). Despite this, evidence for homophilic adhesion in desmosomal cadherins is seen in cell aggregation experiments with both DSG1 and DSC2 (5, 6), although co-expression of both molecules enhanced adhesion relative to either DSG or DSC alone. This agrees with the lower affinity for homophilic adhesion observed in SPR and AUC. Additionally, weak homophilic adhesion has been observed in DSG1 *trans* interactions using single-molecule AFM, with unbinding forces between 37 - 68 pN observed at pulling speeds of 300-6000 nm/s (7). Dissociation constants are tighter or similar for mouse PCDH α 7 EC1-5 ($K_D \sim 2.9 \pm 0.5 \mu\text{M}$ at 25°C from AUC experiments) (8) and PCDH β 6 EC1-4 ($K_D \sim 16.3 \pm 2.1 \mu\text{M}$ at 25°C from AUC experiments) (9), not reported for human PCDH γ B3 EC1-4, but less tight for mouse family members PCDH γ B2 EC1-5 and PCDH γ B5 EC1-4 that form similar complexes ($K_D \sim 21.8 \pm 0.21 \mu\text{M}$ and $K_D \sim 79.1 \pm 4.3 \mu\text{M}$, respectively, at 25°C from AUC experiments) (10).

Video S1. Forced unbending and unbinding of *mm* CDH1 EC1-5. Stretching of the CDH1 *trans* dimer at 0.5 nm/ns (simulation S1d, Table S1, 0 – 33.4 ns) causes soft unbending of the inherent curvature of CDH1 monomers, followed by stiff phase, prior to unbinding of the *trans* interaction. Monomers begin to re-bend immediately after unbinding. Proteins are depicted in ribbon representation (greens), while water molecules and solute ions are not shown for clarity.

Video S2. Dislodging of Trp² residue immediately precedes *mm* CDH1 *trans* dimer separation. Focused view of the stretching of the *trans* CDH1 dimer at 0.5 nm/ns (simulation S1d, Table S1, 0 – 33.4 ns). Dislodging of Trp² (orange) from the hydrophobic pocket of the binding partner is observed. One monomer is shown in surface representation, while the other is shown in ribbon.

Video S3. Forced unbending and unbinding of the *hs* DSG2-DSG2 EC1-5 homodimer. Stretching of the DSG2-DSG2 *trans* dimer at 0.1 nm/ns (simulation S3d, Table S1) results in unbending of the inherent curvature of the DSG2 monomers, followed by a stiff phase, prior to unbinding of the *trans* interaction. Monomers begin to re-bend immediately after unbinding. System depicted as in Video S1. Similar trajectories were observed for the DSG2-DSC1 heterodimer and the DSC1-DSC1 homodimer.

Video S4. Dislodging of Trp² residue immediately precedes *hs* DSG2 *trans* homodimer separation. Focused view of the stretching of the *trans* DSG2 homodimer at 0.1 nm/ns (simulation S3d, Table S1). Dislodging of the Trp² (orange) from the hydrophobic pocket of the binding partner is observed. One monomer is shown in surface representation, while the other is shown in ribbon. Similar trajectories were observed for the DSG2-DSC1 heterodimer and the DSC1-DSC1 homodimer.

Video S5. Forced unbinding of *mm* PCDHβ6 EC1-4. Stretching of the PCDHβ6 *trans* homodimer at 0.1 nm/ns (simulation S7d, Table S1, 0 – 180 ns) results in rupture of the EC1-EC4 interface and the formation of transient intermediates before complete unbinding of the complex. System depicted as in Video S1.

Video S6. Transient interactions during forced unbinding of *mm* PCDHβ6 EC1-4. Close up view of the transient interaction that forms between Arg⁴ (A) and Glu¹⁶⁵ (B) during stretching of the PCDHβ6 *trans* homodimer at 0.1 nm/ns (simulation S7d, Table S1, 0 – 180 ns). Monomer B is shown in bright pink while monomer A is shown in dark red color.

Video S7. Forced unbinding and glycosylation in *hs* PCDHγB3. Location of glycosylation sites in the PCDHγB3 *trans* homodimer during forced stretching at 0.1 nm/ns (simulation S8d, Table S1, 0 – 185.4 ns). Protein is shown in gray ribbon representation, residues that form interactions with each other are shown as magenta spheres, while glycosylation sites are shown as cyan spheres. Glycosylation is not expected to interfere with unbinding pathway.

Table S1. Summary of simulations.

Label	System	t_{sim} (ns)	Type	Start	Speed (nm/ns)	Average Peak Force (pN) ^e	Size (#atoms)	Initial Size (nm ³)
S1a	Linear CDH1	21.2	EQ ^a	–	–	–	321,547	54.9 × 7.5 × 8.2
S1b		3.5	SMD ^c	S1a	10	987.7		
S1c		20	SMD ^c	S1a	1	591.7		
S1d		33.4	SMD ^c	S1a	0.5	408.4		
S1e		40.0	SMD ^c	S1a [†]	0.5	421.7		
S1f		40.0	SMD ^c	S1a [‡]	0.5	414.2		
S2a	Diagonal CDH1	21.2	EQ ^b	–	–	–	2,868,694	43.9 × 22.7 × 29.4
S2b		3.5	SMD ^d	S2a	10	786.9		
S2c		29.8	SMD ^d	S2a	1	666.8		
S2d		47.2	SMD ^d	S2a	0.5	397.2		
S2e		49.6	SMD ^d	S2a [€]	0.5	543.9		
S3a	DSG2-DSG2	21	EQ ^a	–	–	–	429,545	59.9 × 9.0 × 8.3
S3b		5	SMD ^c	S3a	10	1081.0		
S3c		18.2	SMD ^c	S3a	1	453.4		
S3d		175	SMD ^c	S3a	0.1	323.4		
S4a	DSG2-DSC1	21	EQ ^a	–	–	–	558,418	61.2 × 9.6 × 9.9
S4b		2.6	SMD ^c	S4a	10	1010.4		
S4c		45.4	SMD ^c	S4a	1	499.2		
S4d		182	SMD ^c	S4a	0.1	395.7		
S5a	DSC1-DSC1	21	EQ ^a	–	–	–	365,669	60.9 × 8.7 × 7.3
S5b		5.8	SMD ^c	S5a	10	1036.2		
S5c		18.2	SMD ^c	S5a	1	525.6		
S5d		162	SMD ^c	S5a	0.1	419.8		
S6a	PCDH α 7	21.1	EQ ^a	–	–	–	500,917	54.0 × 10.0 × 9.6
S6b		2.4	SMD ^c	S6a	10	1501.4		
S6c		21	SMD ^c	S6a	1	832.2		
S6d		128	SMD ^c	S6a	0.1	394.1		
S7a	PCDH β 6	19.3	EQ ^a	–	–	–	394,722	43.4 × 10.0 × 9.5
S7b		2.3	SMD ^c	S7a	10	1500.8		
S7c		20	SMD ^c	S7a	1	1061.2		
S7d		180	SMD ^c	S7a	0.1	603.3		
S8a	PCDH γ B3	21.1	EQ ^a	–	–	–	335,584	50.0 × 8.4 × 8.4
S8b		3	SMD ^c	S8a	10	1631.3		
S8c		24.6	SMD ^c	S8a	1	944.2		
S8d		185.4	SMD ^c	S8a	0.1	612.6		
S9a	PCDH β 6	21.2	EQ ^a	–	–	–	102,143	22.2 × 8.2 × 6.3
S9b		100	EQ	–	–	–		
Total		1,736						

[†] denotes that simulation S1e started from simulation S1a at 20.2 ns.

[‡] denotes that simulation S1f started from simulation S1a at 19.2 ns.

[€] denotes that simulation S2e started from simulation S2a at 17.2 ns.

a denotes equilibration simulations that consisted of 5,000 steps of minimization, 200 ps of dynamics with protein backbone constraints ($k = 1 \text{ kcal mol}^{-1} \text{ \AA}^{-2}$), 1 ns of free dynamics in the NpT ensemble ($\gamma = 1 \text{ ps}^{-1}$), and 20 ns of free dynamics in the NpT ensemble ($\gamma = 0.1 \text{ ps}^{-1}$).

b denotes equilibration simulations that consisted of 5,000 steps of minimization, 200 ps of dynamics with protein

backbone constraints ($k = 1 \text{ kcal mol}^{-1} \text{ \AA}^{-2}$), 1 ns of free dynamics in the NpT ensemble ($\gamma = 1 \text{ ps}^{-1}$), and 20 ns of free dynamics in the NpT ensemble ($\gamma = 0.1 \text{ ps}^{-1}$) with C-terminal constraints.

c SMD simulations in which C-terminal C_{α} -atoms were attached to independent virtual springs.

d SMD simulations in which C-terminal C_{α} -atoms were attached to independent virtual springs and harmonic constraints were applied.

e The average force peak is calculated from the peak force of stretched virtual springs with a 50 ps running average.

Table S2. List of species and accession numbers of sequences used in multiple sequence alignment analyses

Sequences for CDH1		
Species	Abbreviation	NCBI Accession Number
<i>Homo sapiens</i>	<i>Hs</i>	NP_004351.1
<i>Mus musculus</i>	<i>Mm</i>	NP_033994.1
<i>Gallus gallus</i>	<i>Gg</i>	NP_001034347.3
<i>Anolis carolinensis</i>	<i>Ac</i>	XP_008121673.2
<i>Danio rerio</i>	<i>Dr</i>	NP_571895.1
Sequences for DSG2		
Species	Abbreviation	NCBI Accession Number
<i>Homo sapiens</i>	<i>Hs</i>	NP_001934.2
<i>Mus musculus</i>	<i>Mm</i>	NP_031909.2
<i>Gallus gallus</i>	<i>Gg</i>	XP_426083.5
<i>Anolis carolinensis</i>	<i>Ac</i>	XP_003223578.1
<i>Danio rerio</i>	<i>Dr</i>	XP_005171176.3
Sequences for DSC1		
Species	Abbreviation	NCBI Accession Number
<i>Homo sapiens</i>	<i>Hs</i>	NP_077739.1
<i>Mus musculus</i>	<i>Mm</i>	NP_001278733.1
<i>Gallus gallus</i>	<i>Gg</i>	XP_015138083.2
<i>Anolis carolinensis</i>	<i>Ac</i>	XP_016850634.1
<i>Danio rerio</i>	<i>Dr</i>	NP_001274012.1
Sequences for PCDH α 7		
Species	Abbreviation	NCBI Accession Number
<i>Homo sapiens</i>	<i>Hs</i>	NP_061733.1
<i>Mus musculus</i>	<i>Mm</i>	NP_034087.2
<i>Gallus gallus</i>	<i>Gg</i>	NP_001104607.1
<i>Danio rerio</i>	<i>Dr</i>	XP_021336978.1
Sequences for PCDH β 6		
Species	Abbreviation	NCBI Accession Number
<i>Homo sapiens</i>	<i>Hs</i>	NP_061762.2
<i>Mus musculus</i>	<i>Mm</i>	NP_444361.1
<i>Tricholaema leucomelas</i>	<i>Tl</i>	NXX41767.1
<i>Sceloporus undulatus</i>	<i>Su</i>	NC_056525.1
<i>Thunnus albacares</i>	<i>Ta</i>	XP_044220385.1
Sequences for PCDH γ B3		
Species	Abbreviation	NCBI Accession Number
<i>Homo sapiens</i>	<i>Hs</i>	NP_061747.2
<i>Tursiops truncatus</i>	<i>Tt</i>	XP_033709215.1
<i>Tupaia chinensis</i>	<i>Tc</i>	XP_006156321.1

Table S3. Biophysical parameters for selected cadherins (1–5, 7, 9, 10).

Measurement	CDH1	CDH2 ^a	DSG2	DSG2/DSC1	DSC1	PCDH α 7	PCDH β 6	PCDH γ 3	PCDH γ 2 ^a
K_D AUC μ M	109 \pm 6	7.8 \pm 0.3	433 \pm 102	-	39 \pm 0	2.9 \pm 0.5	16.3 \pm 2.1	-	21.8 \pm 0.2
K_D SPR μ M	-	-	no signal	11.52	no signal	-	-	-	-
Bead Agg	yes	-	no	yes	no	-	-	-	-
Cell Agg	yes	yes	-	-	-	yes	yes	-	-
F_p AFM pN	73 - 157 (1 - 10 nm/s)	30 - 40 (1 - 10 nm/s)	20 - 40 (200 - 5000 nm/s)	-	-	-	-	-	-
F_p SMD pN	414 - 470 (0.5 nm/ns)	-	323.4 (0.1 nm/ns)	395.7 (0.1 nm/ns)	419.8 (0.1 nm/ns)	394.1 (0.1 nm/ns)	603.3 (0.1 nm/ns)	612.6 (0.1 nm/ns)	-
k_{soft} SMD mN/m	3.4 - 3.8	-	9.3	7.1	8.4	-	-	-	-
BSA \AA^2	789.0	750.0	642.2	1002.8	753.6	2011.2	2397.5	1536.5	-

^a Not simulated in the current study.

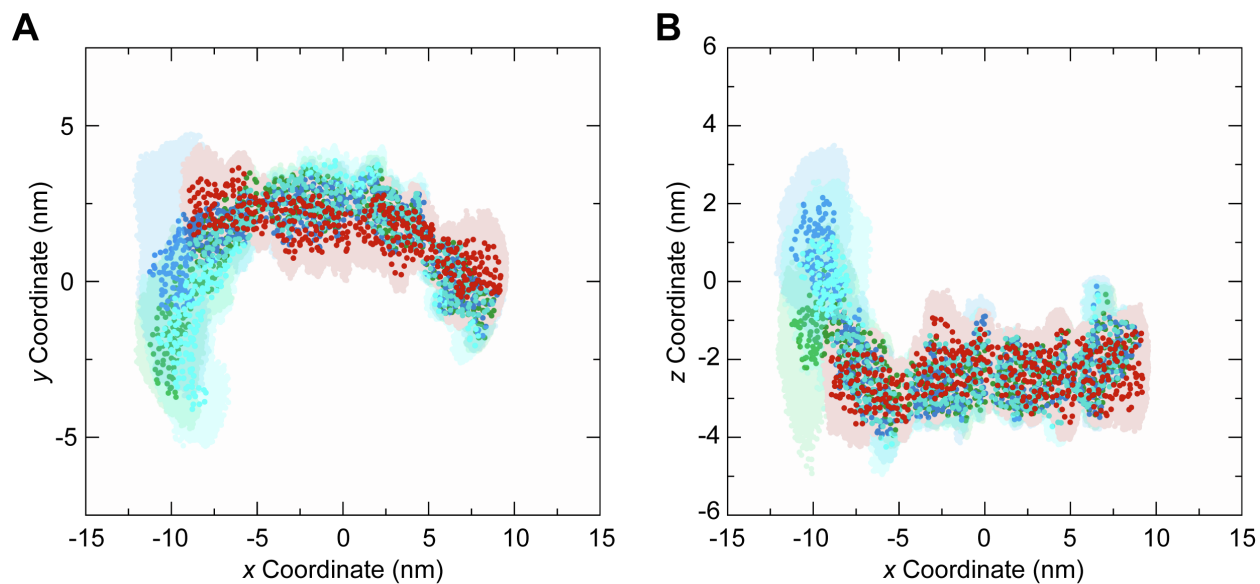


FIGURE S1 Shape of cadherin monomers during equilibration. (A) The x - versus y -coordinates of cadherin monomers during equilibration (CDH1 – green; DSG2 – cyan; DSC1 – blue; PCDHβ6 – red). Circles represent the average location of C_α atoms during equilibration. Shadows show the motion of C_α atoms during equilibrations (every 50 ps; simulations S1a, S3a, S5a, and S9a-b). (B) The x - versus z -coordinates of cadherin monomers during equilibrations shown as in (A).

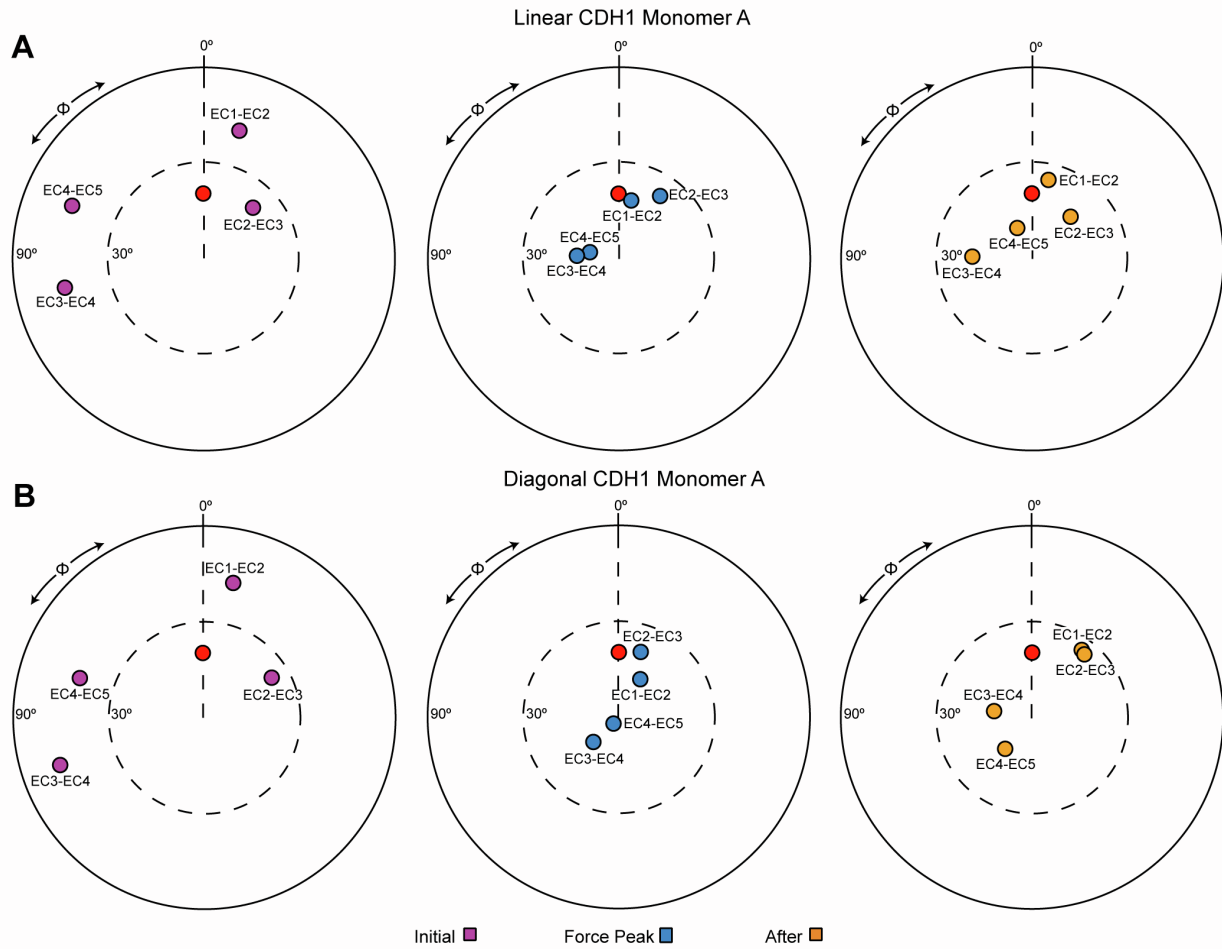


FIGURE S2 Unbending of CDH1 monomers during forced unbinding. (A) The orientation of tandem EC repeats of CDH1 during unbinding at a stretching speed of 0.5 nm/ns (simulation S1d; linear system; Table 1). The N-terminal EC repeat was used as reference and aligned to the z -axis, and the principal axis of the subsequent C-terminal EC was projected in the x - y plane (colored circles). The structure of CDH23 EC1-2 (PDB: 2WHV; red circle) was used to define $\phi = 0^\circ$. Panels show the tandem EC orientation at the initial conformation (purple, left), at the force peak (blue, middle), and shortly after unbinding (yellow, right) during simulation S1d. (B) Snapshots of the orientation of tandem EC repeats of CDH1 during unbinding at a stretching speed of 0.5 nm/ns (simulation S2d; diagonal system) shown as in (A). Both systems show unbending of CDH1 monomers, until unbinding, followed by partial re-bending.

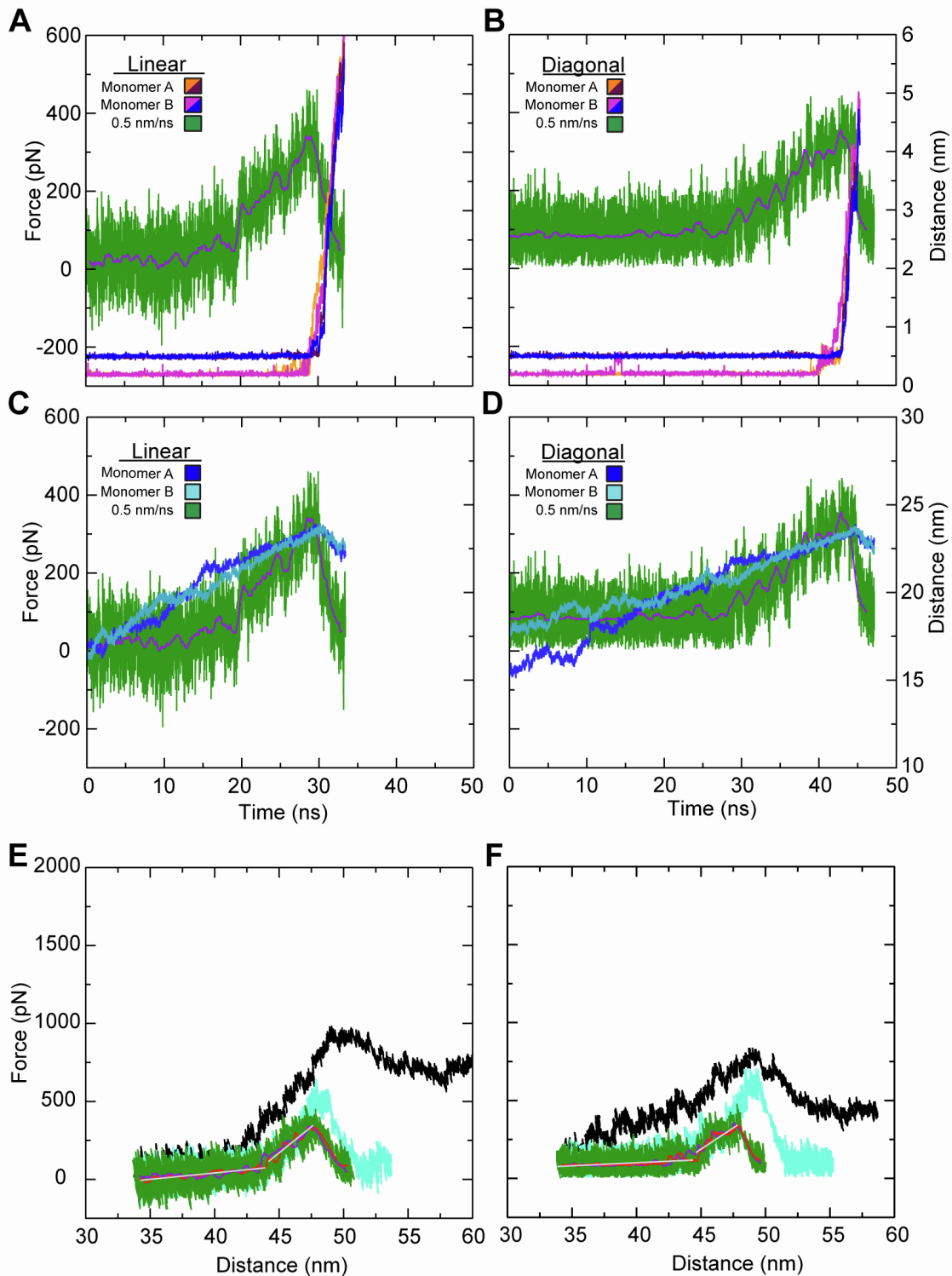


FIGURE S3 Elasticity and interactions during simulated forced unbinding of CDH1 dimers. (A) Force versus time plot for the linear constant velocity stretching of the CDH1 dimer (monomers A and B) at 0.5 nm/ns (simulation S1d, green; 1 ns running average shown in purple). Overlaid are the distances for Trp² H_ε (A) – Asp⁹⁰ O (B) (orange), Asp¹ C_γ (A) – Asn²⁷ N_ε (B) (maroon), Trp² H_ε (B) – Asp⁹⁰ O (A) (purple), and Asp¹ C_γ (B) – Asn²⁷ N_ε (A) (blue) during simulation S1d. Rupture of these interactions correlates with unbinding force peaks. (B) Force versus time plot for the diagonal system as shown in (A). Rupture of these interactions correlates with unbinding force peaks. (C) Force

versus end-to-end distance plot for the linear system shown as in (A) along with the CDH1 monomer N- to C-terminal distances (blues) for each monomer during the S1d simulation. (D) Force versus time plot for the diagonal constant velocity stretching of the CDH1 dimer at 0.5 nm/ns (simulation S2d) shown as in (A). In both the linear and diagonal systems, the monomers straightened until unbinding before re-bending. (E-F) Force versus end-to-end distance plot for the monomer not shown in Fig. 2 in constant velocity stretching of the two classical cadherin simulation systems at 10 nm/ns (simulations S1b and S2b, black), 1 nm/ns (simulations S1c and S2c, cyan), and 0.5 nm/ns (simulations S1d and S2d, green; 1 ns running averages shown in red for one monomer and purple for the other; gray lines are linear fits used to determine elasticity). Forces monitored for both monomers at the slowest stretching speed were similar.

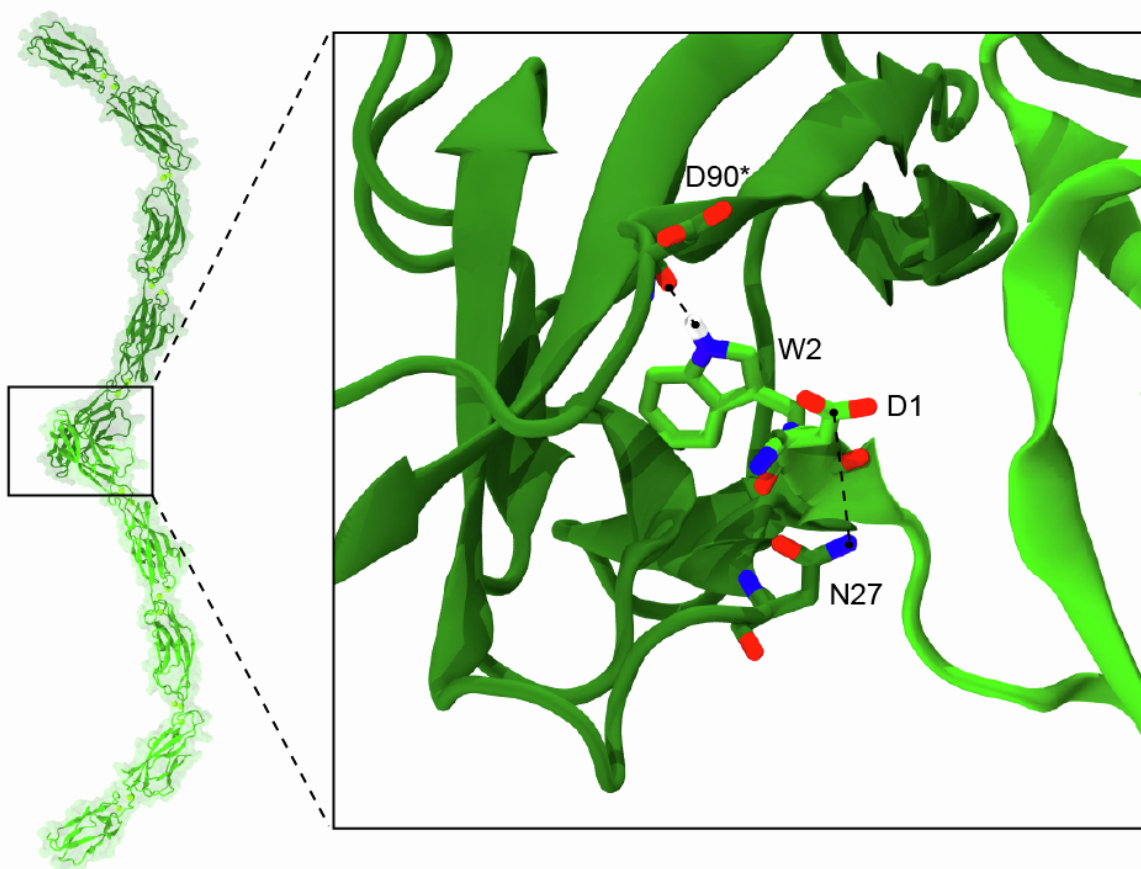
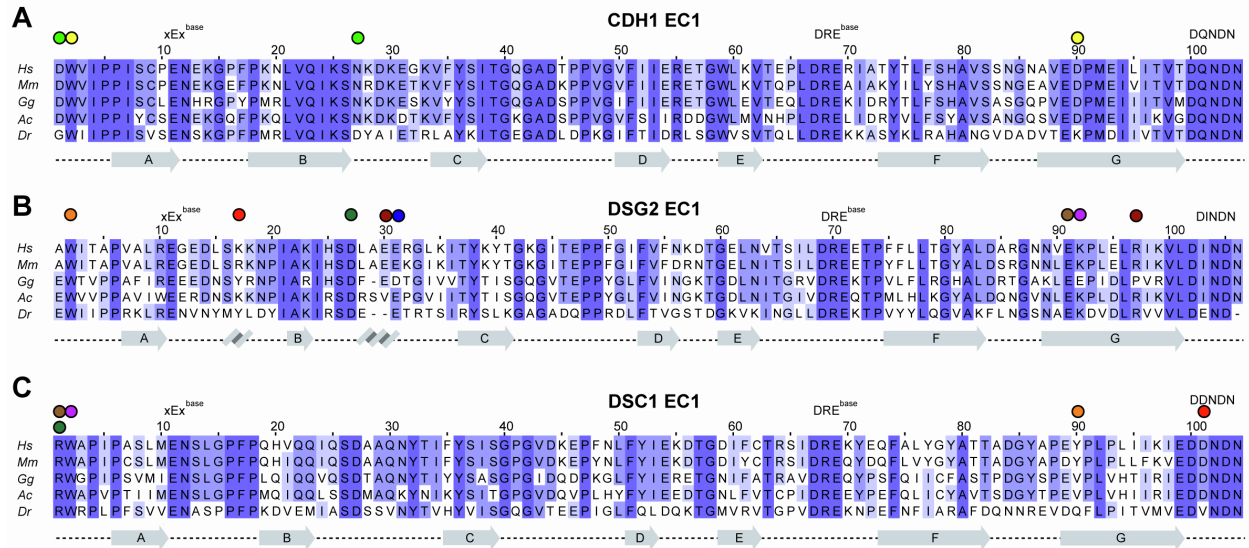
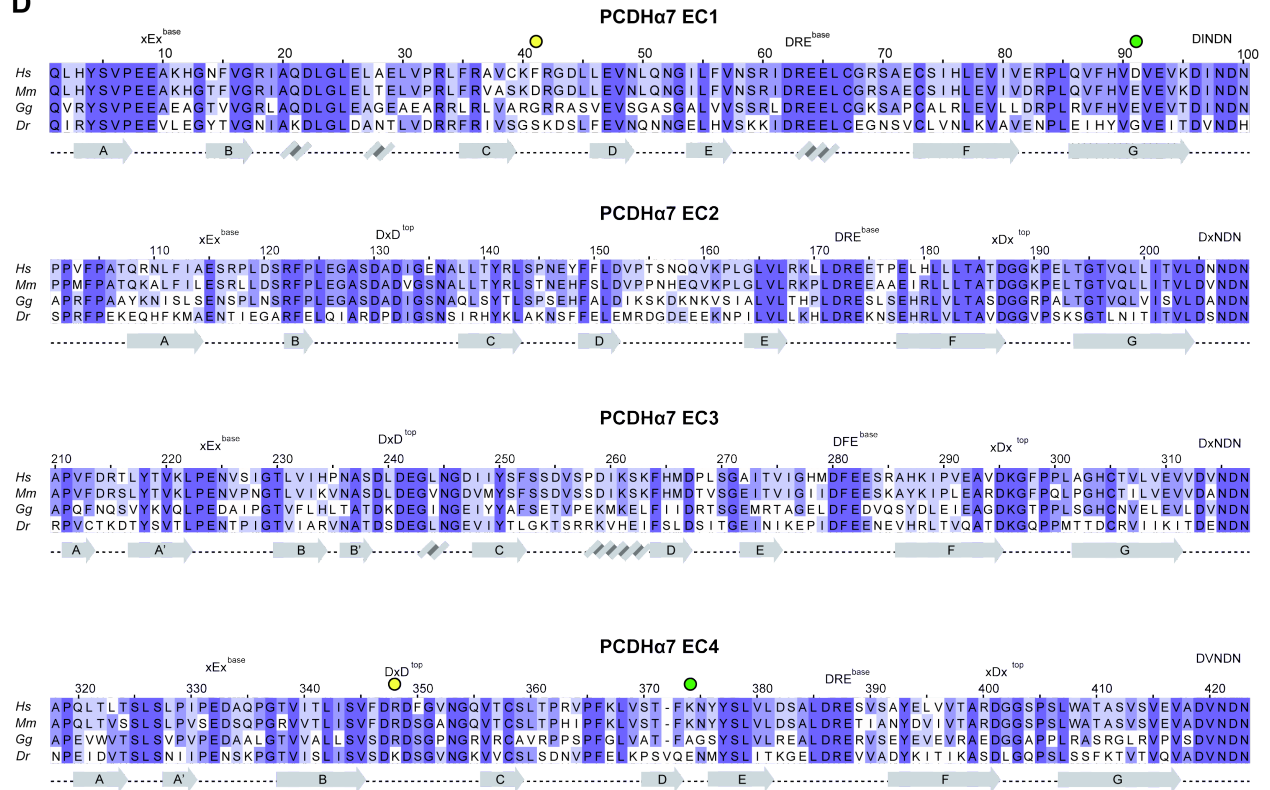
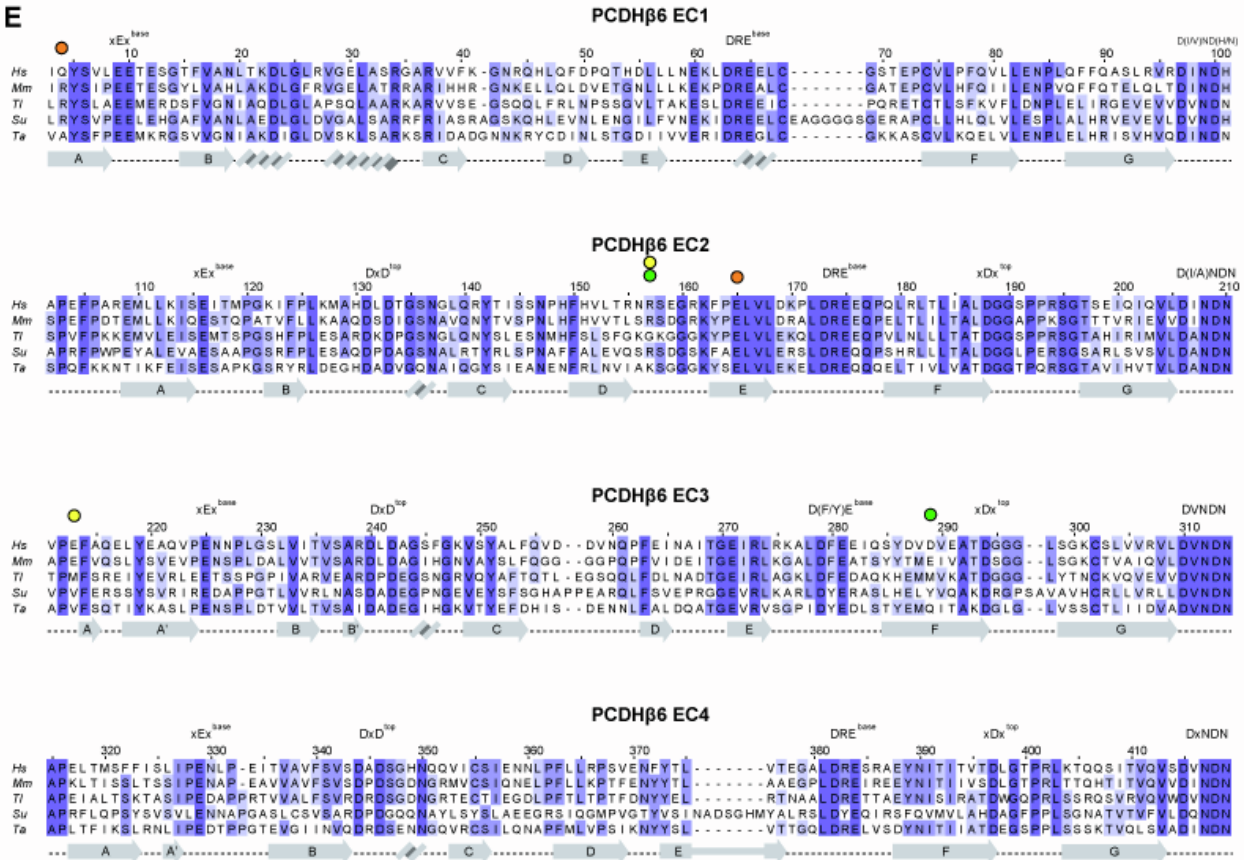


FIGURE S4 Interactions within the *trans* interface of CDH1 systems. Distances between Trp² H_ε – Asp⁹⁰ O and Asp¹ C_γ – Asn²⁷ N_ε were used to monitor unbinding of CDH1 monomers during SMD simulations as seen in Fig. S3 *A* and *B*. Asterisk denotes the backbone O of Asp⁹⁰ is involved in the hydrogen bonding with Trp².



D

E



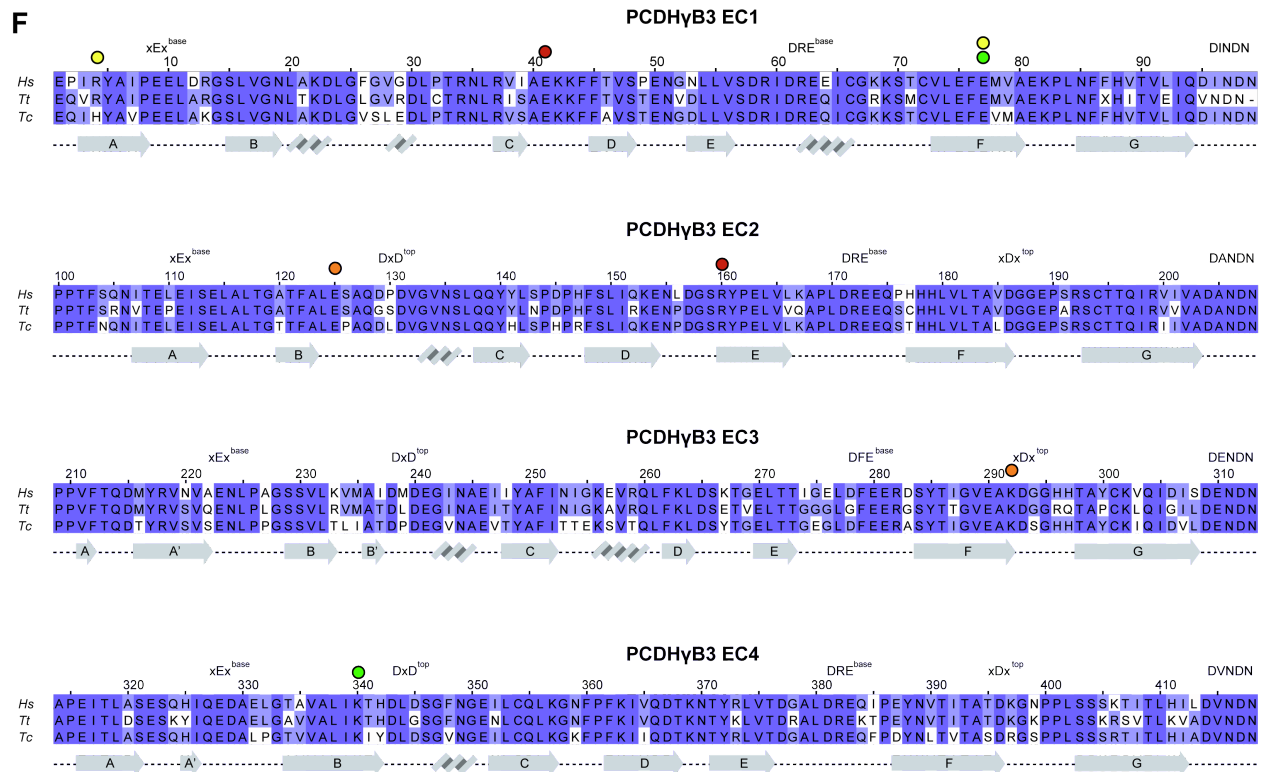


FIGURE S5 Sequence alignment of cadherin binding domains. (A) Multiple sequence alignment of CDH1 EC1 from five species (Table S2). Alignment is colored by sequence similarity with white being the lowest and blue being the highest. Ca^{2+} -binding motifs are labeled on top of each alignment. Selected *trans*-interacting residues are highlight by colored circles. Secondary structure elements are displayed below alignments. Species chosen by availability and taxonomical diversity. (B) Multiple sequence alignment of DSG2 EC1 from five species (Table S2). Displayed as in (A). Selected heterophilic *trans*-interacting residues highlighted by colored circles. (C) Multiple sequence alignment of DSC1 EC1 from five species (Table S2). Displayed as in (A). Selected heterophilic *trans*-interacting residues highlighted by colored circles. (D) Multiple sequence alignment of PCDHa7 EC1-4 from four species (Table S2). Displayed as in (A). Selected *trans*-interacting residues highlighted by colored circles. (E) Multiple sequence alignment of PCDH β 6 EC1-4 from five species (Table S2). Displayed as in (A). Selected *trans*-interacting residues highlighted by colored circles. (F) Multiple sequence alignment of PCDH γ B3 EC1-4 from three species (Table S2). Displayed as in (A). Selected *trans*-interacting residues highlighted by colored circles.

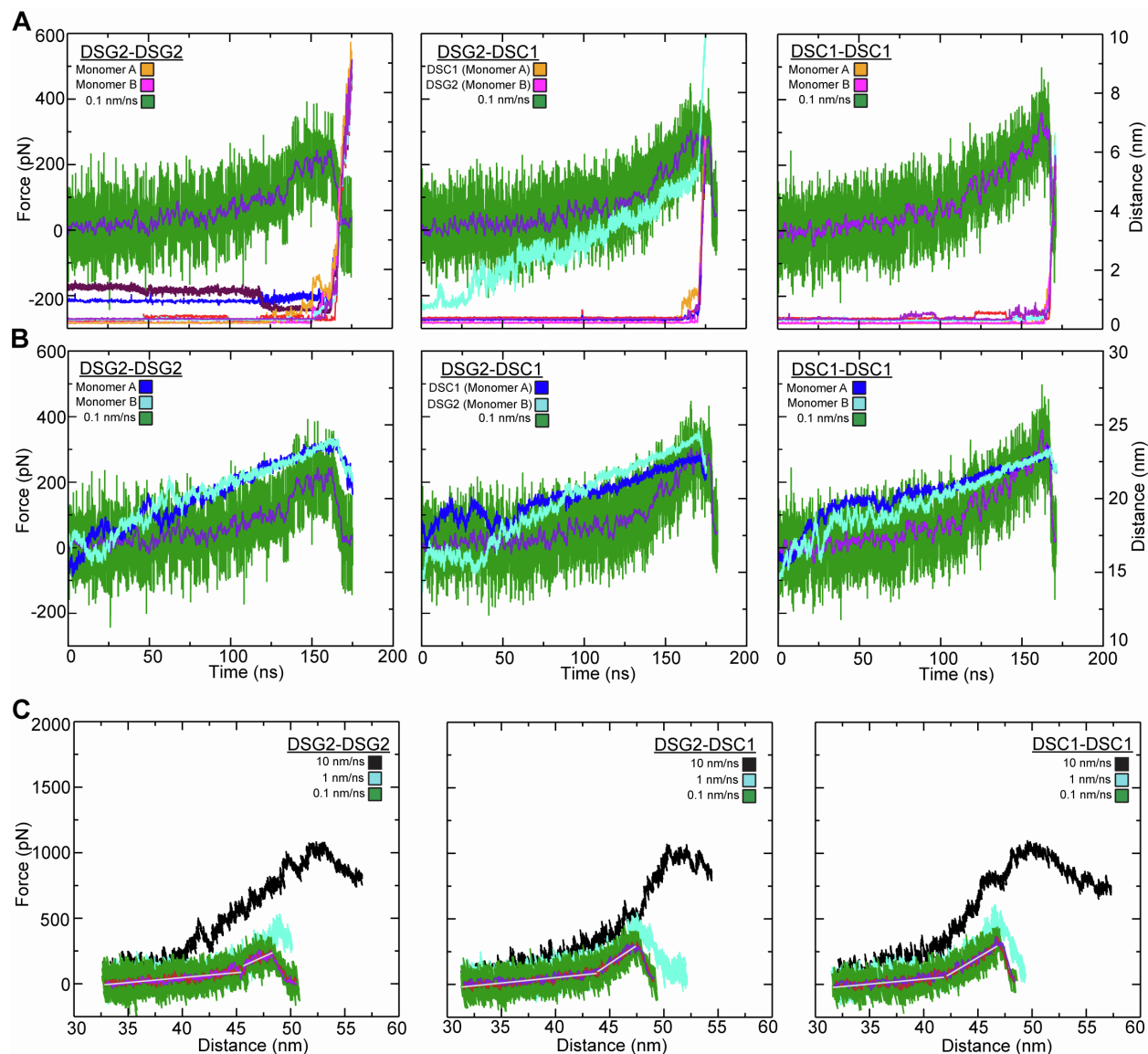


FIGURE S6 Elasticity and interactions during simulated forced unbinding of desmosomal dimers. (A) Force versus time plot for the constant velocity stretching of the DSG2-DSG2, DSG2-DSC1, and DSC1-DSC1 dimers (monomers A and B) at 0.1 nm/ns (S3d, S4d, S5d, green; 1 ns running average shown in purple). Trp² H_ε (A) – Lys⁹² O (B) (orange) and Trp² H_ε (B) – Lys⁹² O (A) (purple), Trp² (A) H_ε – Lys⁹² O (B) (orange) and Trp² H_ε (B) – Tyr⁹⁰ O (A) (purple), and Trp² H_ε (A) – Tyr⁹⁰ O (B) (orange) and Trp² H_ε (B) – Tyr⁹⁰ O (A) (purple) distances are shown for DSG2-DSG2, DSG2-DSC1, and DSC1-DSC1, respectively. Rupture of these interactions correlates with unbinding force peaks. In the first panel, the initial salt-bridge interaction between Arg⁹⁷ (A) – Glu³⁰ (B) (blue) ruptures at ~120 ns and is replaced with a new interaction between Arg⁹⁷ (A) – Glu³¹ (B) (maroon) measured between the center of mass of each residue. Second panel details the salt-bridge interaction that formed during equilibration between DSC1 Asp¹⁰¹ – DSG2 Lys¹⁷ (cyan) measured between the center of mass of each residue. For all three panels, the remaining curves correspond to the *trans* interactions shown in Fig. S7 with respective colors and measured between atoms indicated in Fig. S7. (B) Force versus time plot for the systems shown as in (A). Overlaid are the monomer N- to C-terminal distances (blues) for each monomer during the respective simulations. (C) Force versus end-to-end distance plots for the monomer not shown in Fig. 3 in constant velocity stretching of the three simulation systems at 10 nm/ns (S3b, S4b, S5b, black), 1 nm/ns (S3c, S4c, S5c, cyan), and 0.1 nm/ns (S3d, S4d, S5d, green; 1 ns running averages shown in red for one monomer and purple for the other; gray lines are linear fits used to determine elasticity). Forces monitored for both monomers at the slowest stretching speed were similar as expected.

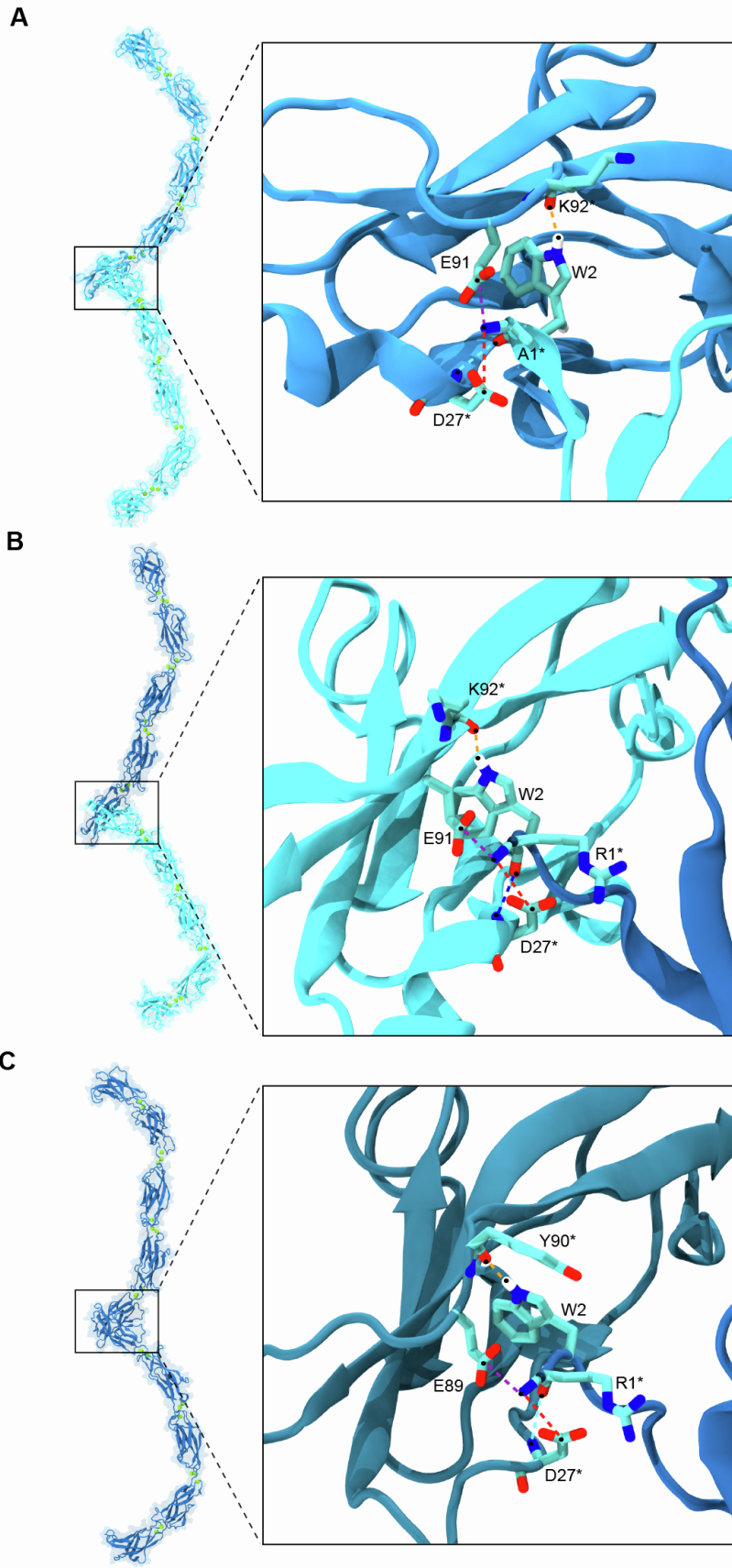


FIGURE S7 Interactions that form the *trans* interface in the three desmosomal systems. (A) In the DSG2-DSG2 *trans* interface, the Trp² indole nitrogen forms a hydrogen bond with the Lys⁹² backbone oxygen on the opposite monomer (orange). Other residues at the interface contribute to a network of interactions that persist until the monomers are pulled apart (Fig. S6 A), including Glu⁹¹ C_δ (A) – Ala¹ N (B) (purple), Ala¹ O (B) – Asp²⁷ N (A) (cyan), and Asp²⁷ C_γ (A) – Ala¹ N (B) (red). (B) In the DSG2-DSC1 *trans* interface, the Trp² indole nitrogen forms a hydrogen bond with the Lys⁹² backbone oxygen on the opposite monomer (orange) in DSG2, or with a Tyr⁹⁰ in DSC2. Other residues at the interface contribute to a network of interactions that persist until the monomers are pulled apart (Fig. S6 A), including Glu⁹¹ C_δ (B) – Arg¹ N (A) (purple), Arg¹ O (A) – Asp²⁷ N (B) (blue), and Asp²⁷ C_γ (B) – Arg¹ N (A) (red). (C) In the DSC1-DSC1 *trans* interface, the Trp² indole nitrogen forms a hydrogen bond with the Tyr⁹⁰ backbone oxygen on the opposite monomer (orange). Other residues at the interface contribute to a network of interactions that persist until the monomers are pulled apart (Fig. S6 A), including Glu⁸⁹ C_δ (B) – Arg¹ N (A) (purple), Arg¹ O (A) – Asp²⁷ N (B) (cyan), and Asp²⁷ C_γ (B) – Arg¹ N (A) (red).

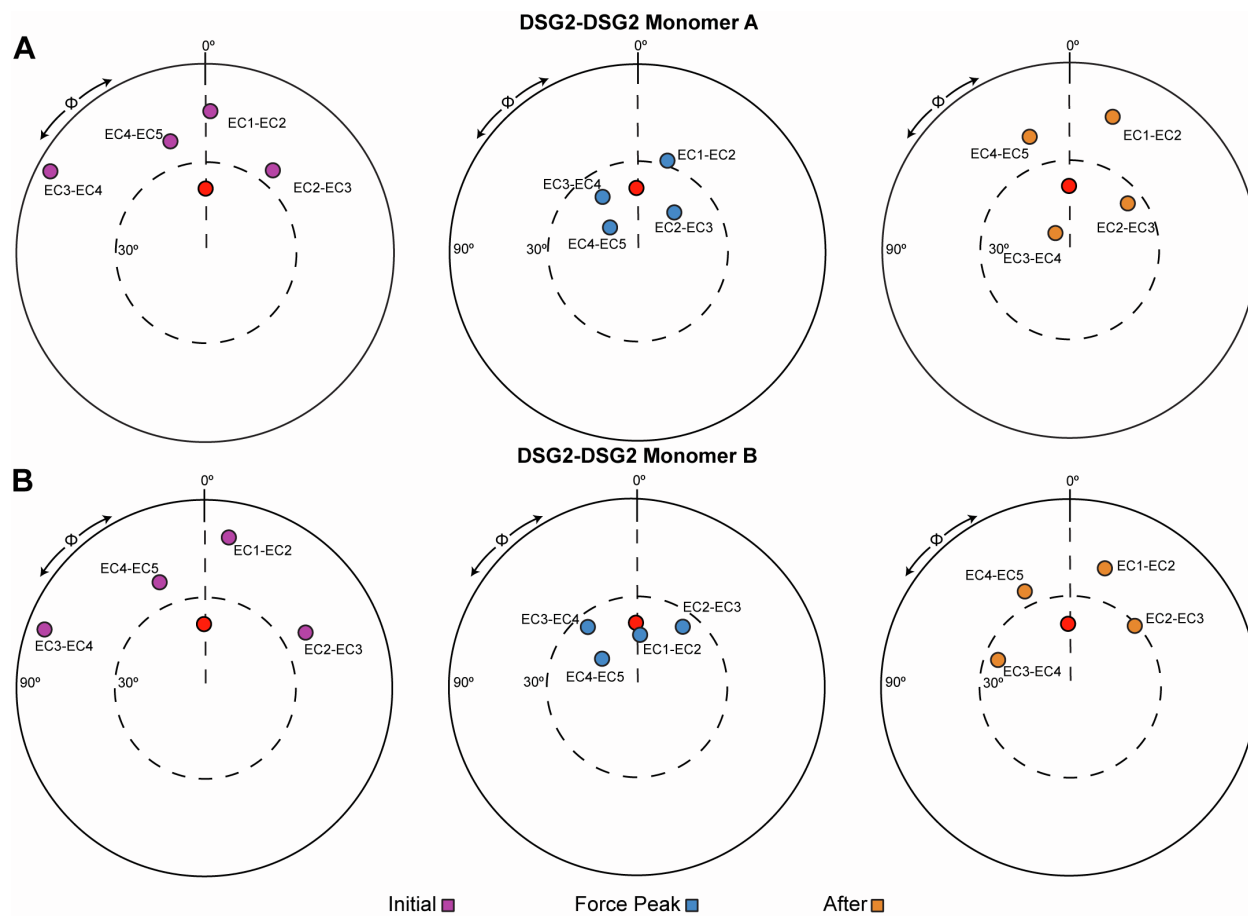


FIGURE S8 Unbending of DSG2-DSG2 dimers during forced unbinding. The orientation of tandem EC repeats of DSG2 monomer A (*A*) and monomer B (*B*) during unbinding at a stretching speed of 0.1 nm/ns (simulation S3d; Table 1). The N-terminal EC repeat was used as reference and aligned to the z -axis, and the principal axis of the subsequent C-terminal EC was projected in the x - y plane (colored circles). The structure of CDH23 EC1-2 (PDB: 2WHV; red circle) was used to define $\varphi = 0^\circ$. Panels show the tandem EC orientation at the initial conformation (purple, left), at the force peak (blue, middle), and shortly after unbinding (yellow, right) during simulation S3d. Unbending is followed by partial re-bending shortly after unbinding.

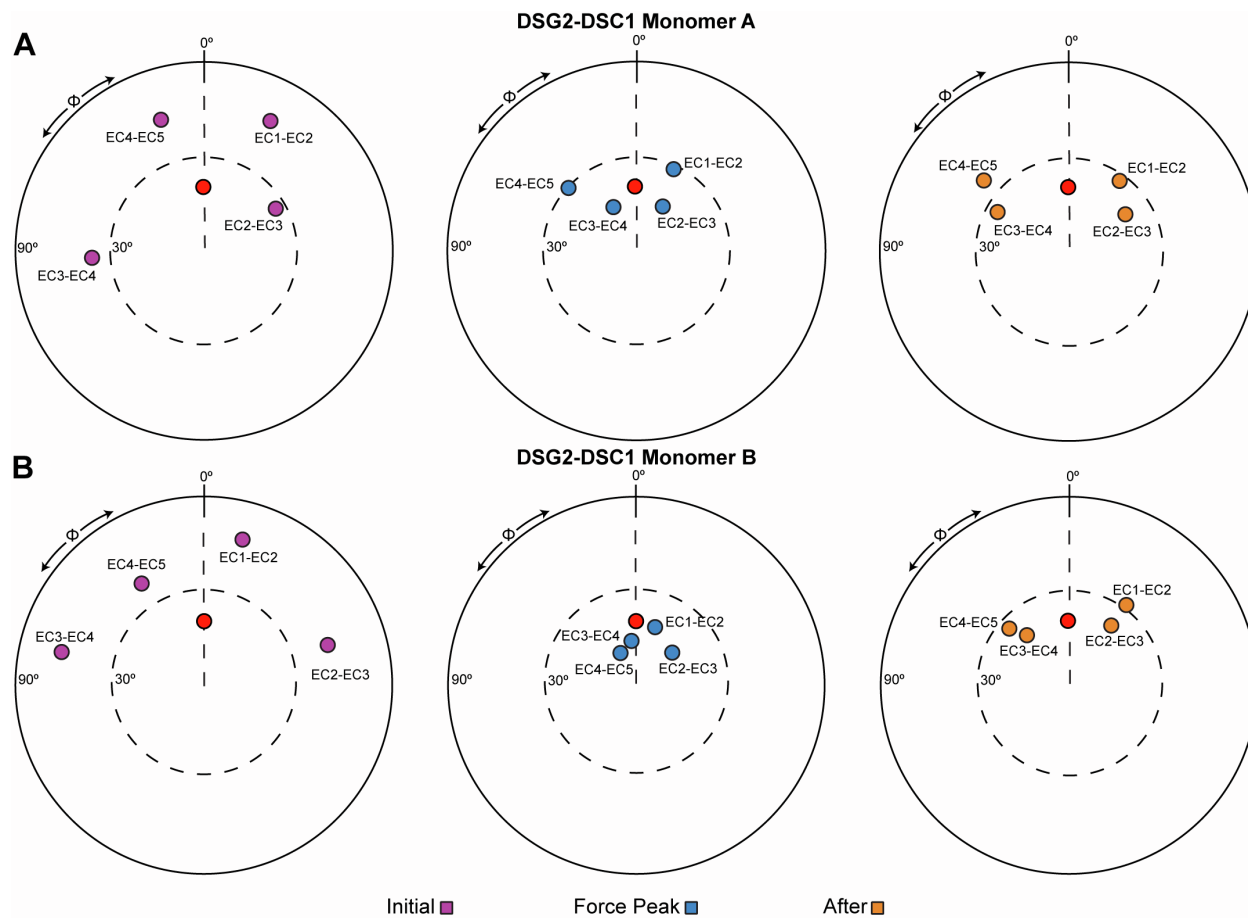


FIGURE S9 Unbending of DSG2-DSC1 dimers during forced unbinding. The orientation of tandem EC repeats of DSC1 (*A*) and DSG2 (*B*) during unbinding at a stretching speed of 0.1 nm/ns (simulation S4d; Table 1). The N-terminal EC repeat was used as reference and aligned to the z -axis, and the principal axis of the subsequent C-terminal EC was projected in the x - y plane (colored circles). The structure of CDH23 EC1-2 (PDB: 2WHV; red circle) was used to define $\varphi = 0^\circ$. Panels show the tandem EC orientation at the initial conformation (purple, left), at the force peak (blue, middle), and shortly after unbinding (yellow, right) during simulation S4d. Unbending is followed by partial re-bending shortly after unbinding.

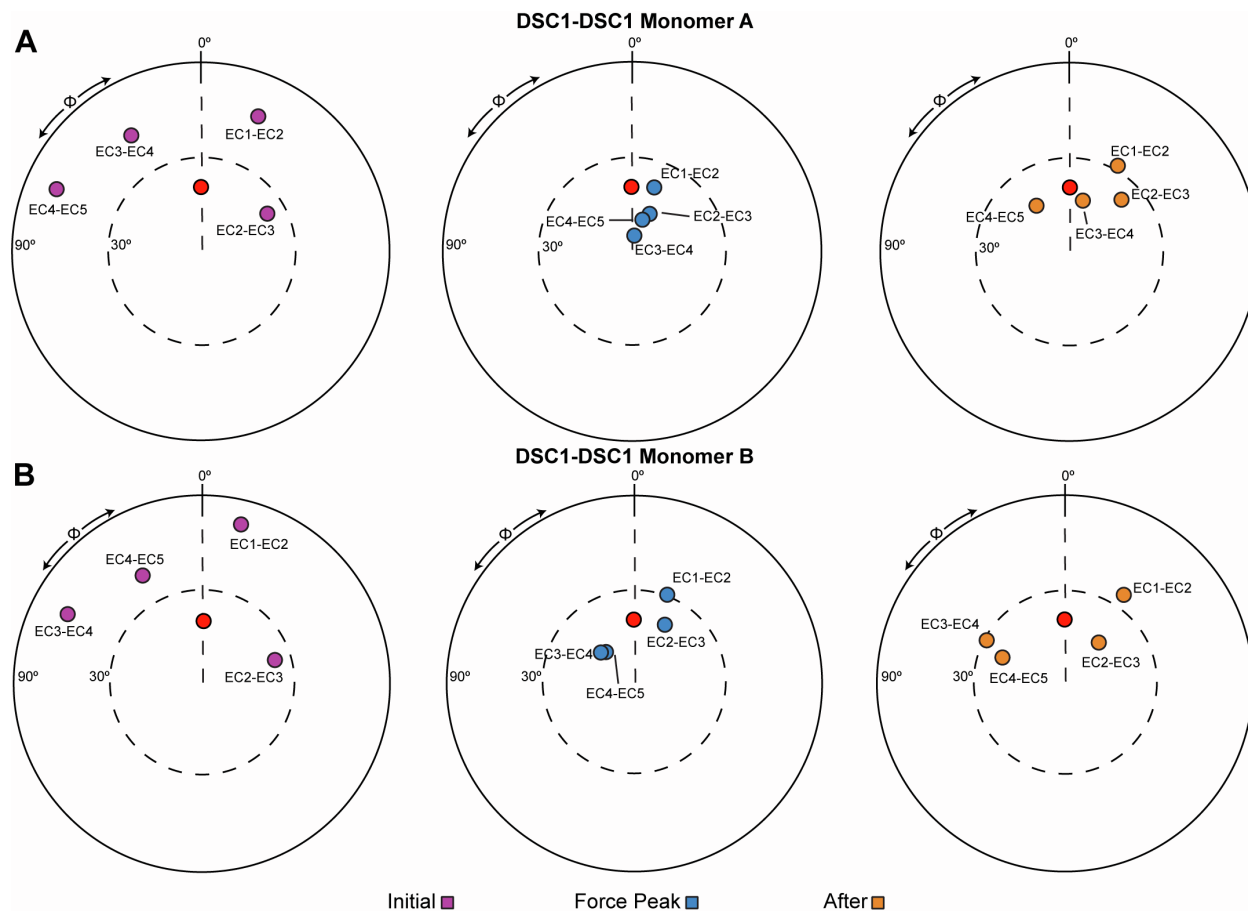


FIGURE S10 Unbending of DSC1-DSC1 dimers during forced unbinding. The orientation of tandem EC repeats of DSC1 monomer A (*A*) and monomer B (*B*) during unbinding at a stretching speed of 0.1 nm/ns (simulation S5d; Table 1). The N-terminal EC repeat was used as reference and aligned to the z -axis, and the principal axis of the subsequent C-terminal EC was projected in the x - y plane (colored circles). The structure of CDH23 EC1-2 (PDB: 2WHV; red circle) was used to define $\varphi = 0^\circ$. Panels show the tandem EC orientation at the initial conformation (purple, left), at the force peak (blue, middle), and shortly after unbinding (yellow, right) during simulation S5d. Unbending is followed by partial re-bending shortly after unbinding.

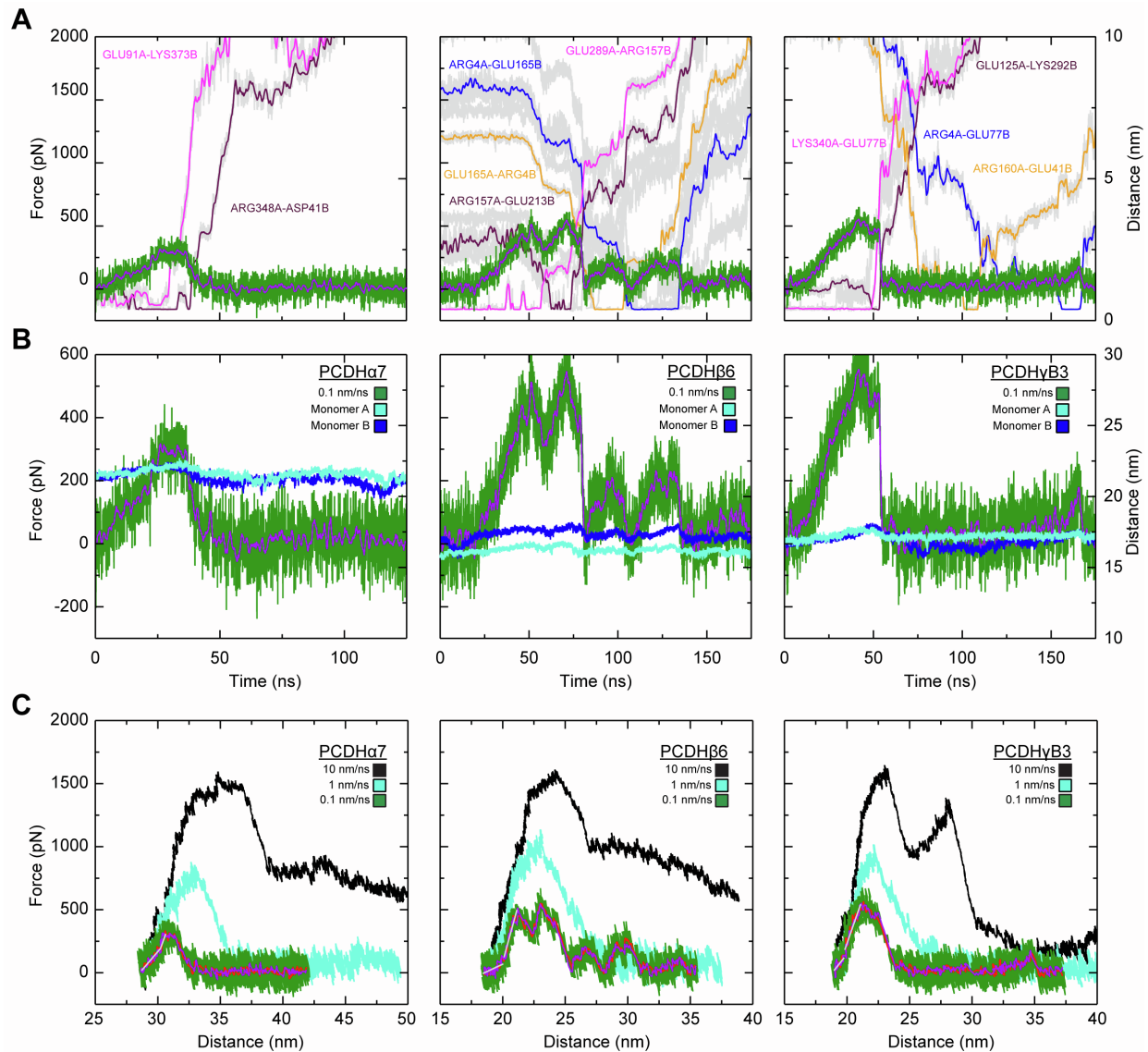
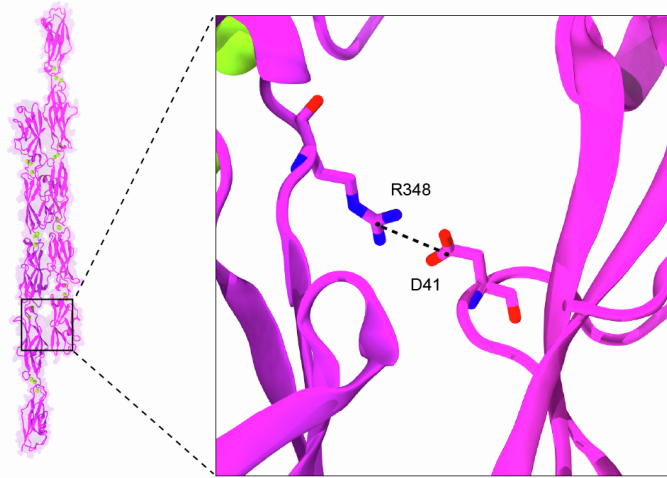


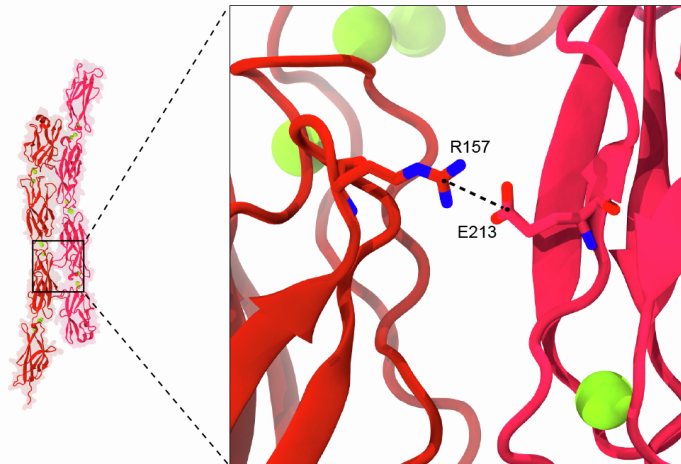
FIGURE S11 Elasticity and interactions during simulated forced unbinding of clustered PCDH dimers. (A) Force versus time plot for constant velocity stretching of the PCDH α 7, PCDH β 6, and PCDH γ B3 dimers (monomers A and B) at 0.1 nm/ns (S6d, S7d, S8d, green; 1 ns running average shown in purple) along with distance between the residues forming salt-bridge interactions (shown in gray). Rupture of these interactions correlates with unbinding force peaks. Left panel shows salt bridges Glu⁹¹ C δ (A) – Lys³⁷³ N ζ (B) (1 ns running average shown in magenta) and Arg³⁴⁸ C ζ (A) – Asp⁴¹ C γ (B) (maroon) that break as force reaches its maximum value during unbinding of PCDH α 7 homodimer. Middle panel shows various salt-bridges that form during the unbinding of PCDH β 6 resulting in multiple force peaks. Initial salt bridge Glu²⁸⁹ C δ (A) – Arg¹⁵⁷ C ζ (B) (magenta) is broken at the first force peak as a new salt bridge Arg¹⁵⁷ C ζ (A) – Glu²¹³ C δ (B) (maroon) is formed giving rise to the next force peak. As this interaction breaks, a new salt bridge, Glu¹⁶⁵ C δ (A) – Arg⁴ C ζ (B) (orange) is formed that breaks just as the force peaks again and as a new salt bridge between Arg⁴ C ζ (A) and Glu⁷⁷ C δ (B) (blue) forms. This salt bridge eventually breaks off as the monomers separate. Right panel shows the initial salt bridge Lys³⁴⁰ N ζ (A) – Glu⁷⁷ C δ (B) of PCDH γ B3 (magenta) broken as the force peaks and a new salt bridge, Glu¹²⁵ C δ (A) – Lys²⁹² N ζ (B) (maroon) is formed transiently, which quickly breaks off within \sim 5 ns. Two more salt bridges, Arg¹⁶⁰ C ζ (A) – Glu⁴¹ C δ (B) (orange) and Arg¹⁶⁰ C ζ (A) – Glu⁴¹ C δ (B) (blue) that form and break as unbinding force rises and falls twice. (B) Force versus time plot for the systems shown as in (A). Overlaid are the monomer N- to C-terminal distances (blues) for each monomer during the respective simulations. (C) Force versus end-to-end distance plots for the monomer not shown in Fig. 4 in constant velocity stretching of the three simulation systems at 10 nm/ns (S6b, S7b, S8b, black), 1 nm/ns (S6c, S7c, S8c, cyan),

and 0.1 nm/ns (S6d, S7d, S8d, green; 1 ns running averages shown in red for one of the monomers and in purple for the other; gray lines are linear fits used to determine elasticity). Forces monitored for both monomers at the slowest stretching speed were similar as expected.

A



B



C

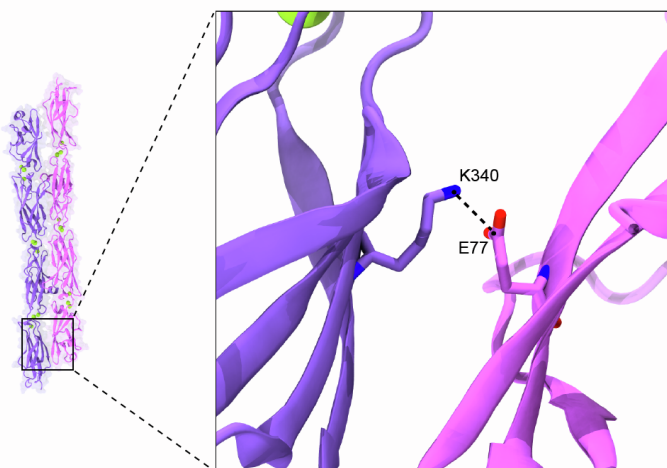


FIGURE S12 Interactions that break during unbinding of clustered PCDH systems. (A) Salt-bridge interaction Arg³⁴⁸ C_ζ (A) – Asp⁴¹ C_γ in the PCDH α 7 *trans* dimeric interface. (B) Salt-bridge interaction Arg¹⁵⁷ C_ζ (A) – Glu²¹³ C_δ (B) in the PCDH β 6 *trans* dimeric interface. (C) Salt bridge interaction Lys³⁴⁰ N_ζ (A) – Glu⁷⁷ C_δ (B) in the PCDH γ B3 interface. These salt-bridges break as the largest force peaks diminish in three simulations of PCDH systems at a stretching speed of 0.1 nm/ns.

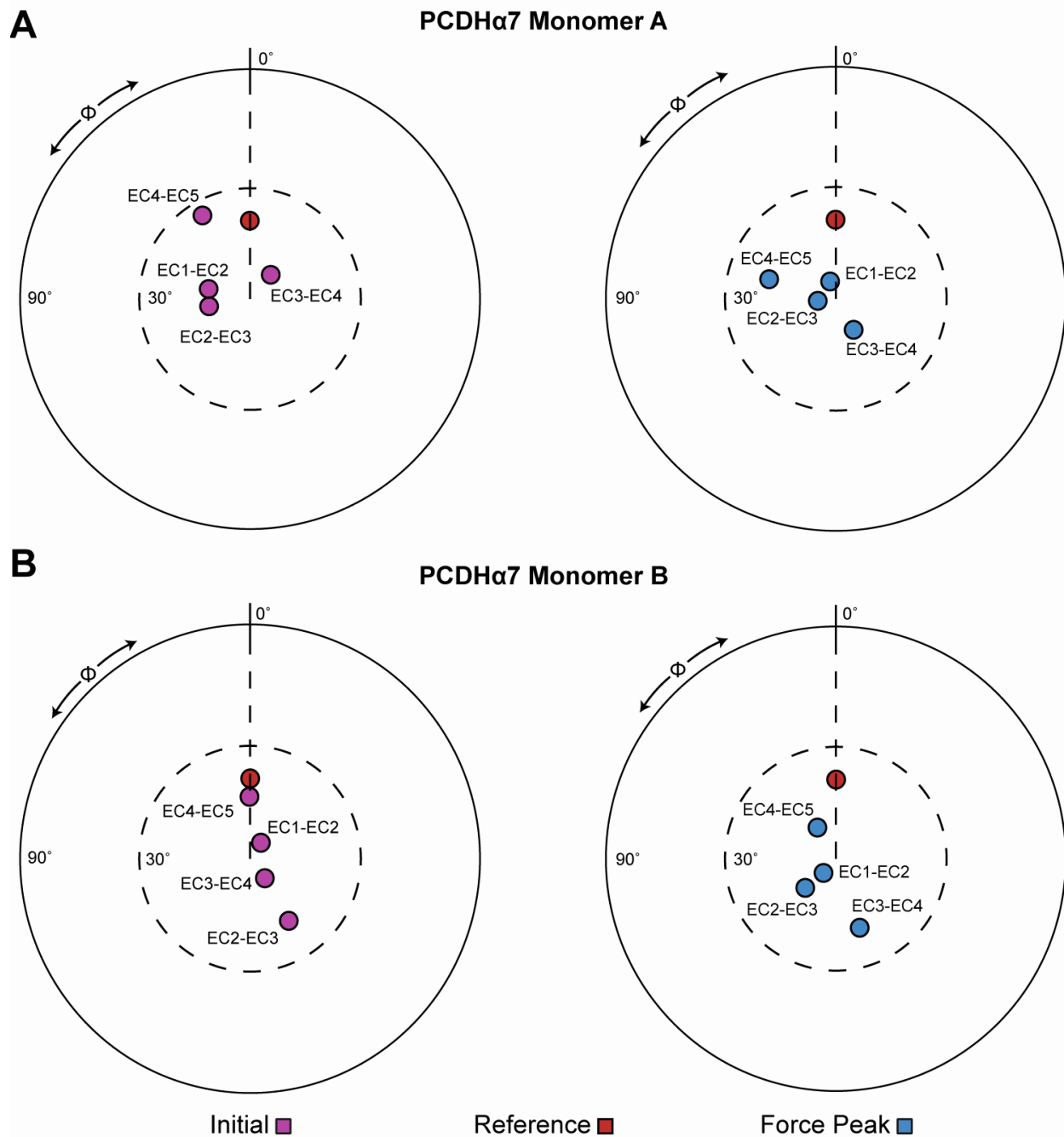


FIGURE S13 Orientation of EC repeats for the PCDH α 7 dimer during forced unbinding. The orientation of tandem EC repeats of PCDH α 7 monomer A (A) and monomer B (B) during unbinding at a stretching speed of 0.1 nm/ns (S6d; Table 1). The N-terminal EC repeat was used as reference and aligned to the z-axis, and the principal axis of the subsequent C-terminal EC was projected in the x - y plane (colored circles). The structure of CDH23 EC1-2 (PDB: 2WHV; red circle) was used to define $\phi = 0^\circ$. Panels show the tandem EC orientation at the initial conformation (purple, left) and at the force peak (blue, right).

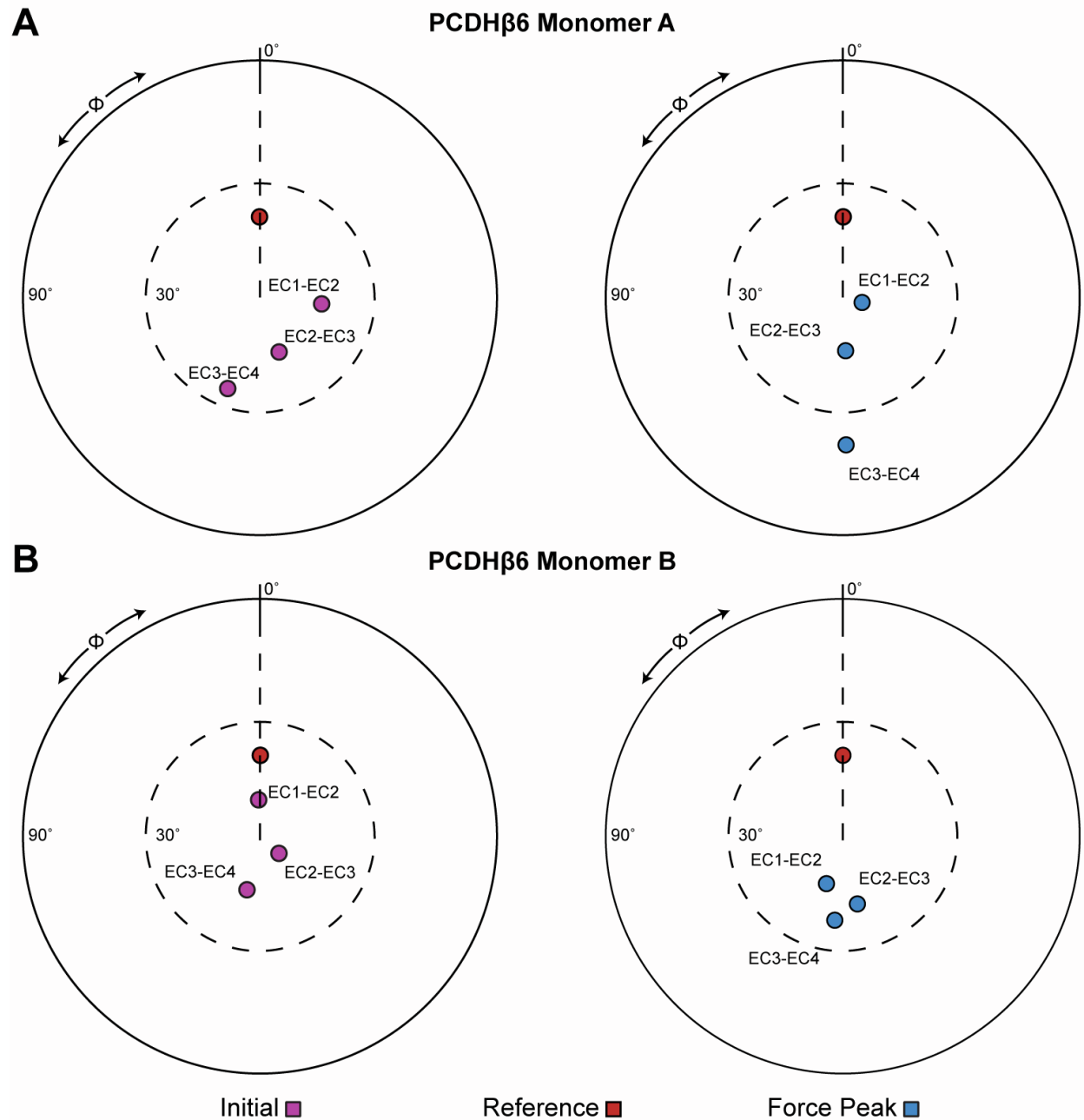


FIGURE S14 Orientation of EC repeats for the PCDH β 6 dimer during forced unbinding. The orientation of tandem EC repeats of PCDH β 6 monomer A (*A*) and monomer B (*B*) during unbinding at a stretching speed of 0.1 nm/ns (S7d; Table 1). The N-terminal EC repeat was used as reference and aligned to the z -axis, and the principal axis of the subsequent C-terminal EC was projected in the x - y plane (colored circles). The structure of CDH23 EC1-2 (PDB: 2WHV; red circle) was used to define $\phi = 0^\circ$. Panels show the tandem EC orientation at the initial conformation (purple, left) and at the force peak (blue, right).

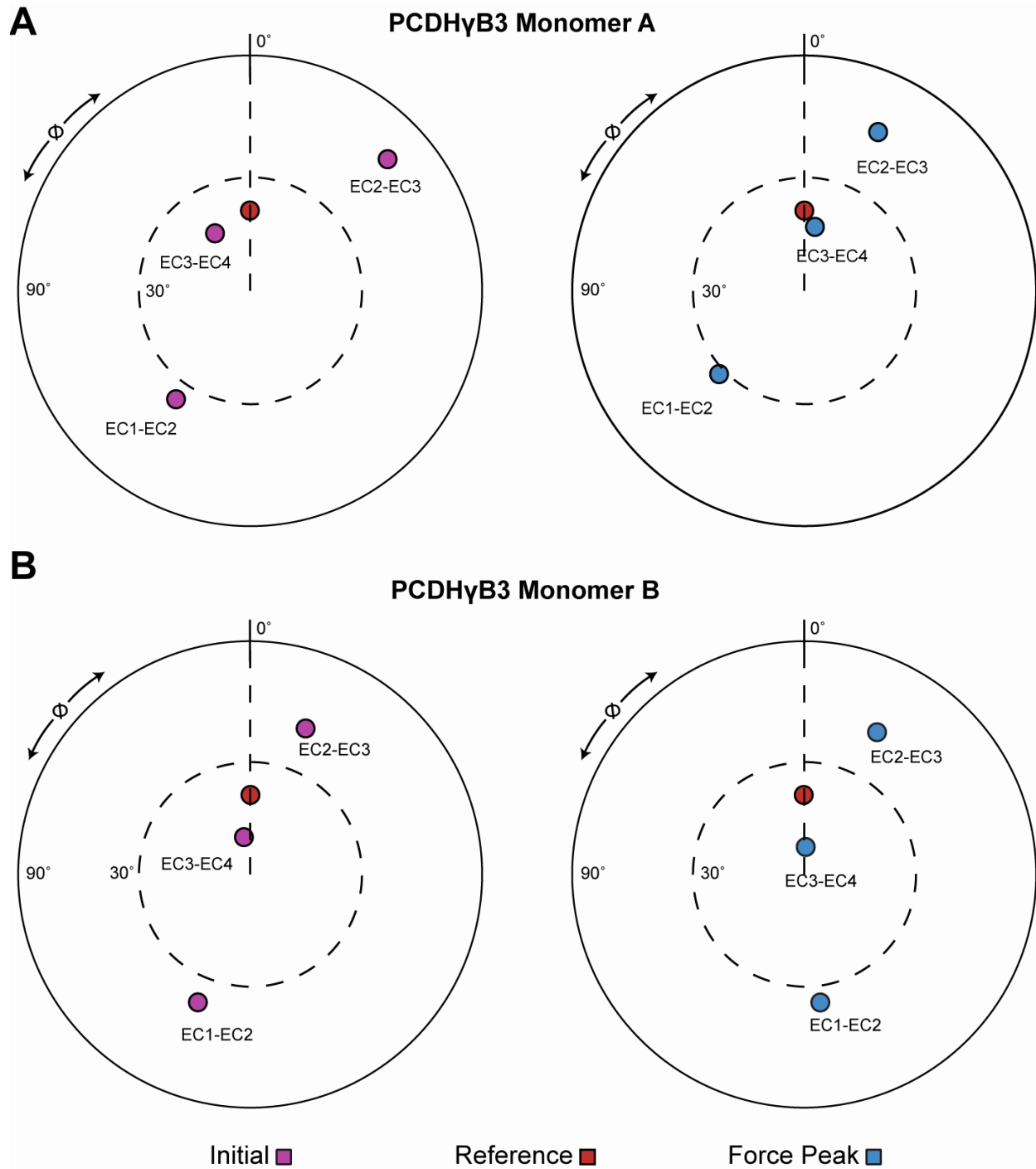


FIGURE S15 Orientation of EC repeats for the PCDH γ B3 dimer during forced unbinding. The orientation of tandem EC repeats of PCDH γ B3 monomer A (*A*) and monomer B (*B*) during unbinding at a stretching speed of 0.1 nm/ns (S8d; Table 1). The N-terminal EC repeat was used as reference and aligned to the z -axis, and the principal axis of the subsequent C-terminal EC was projected in the x - y plane (colored circles). The structure of CDH23 EC1-2 (PDB: 2WHV; red circle) was used to define $\phi = 0^\circ$. Panels show the tandem EC orientation at the initial conformation (purple, left) and at the force peak (blue, right).

SUPPORTING REFERENCES

1. Katsamba, P., K. Carroll, G. Ahlsen, F. Bahna, J. Vendome, S. Posy, M. Rajebhosale, S. Price, T.M. Jessell, A. Ben-Shaul, L. Shapiro, and B.H. Honig. 2009. Linking molecular affinity and cellular specificity in cadherin-mediated adhesion. *Proc. Natl. Acad. Sci. U. S. A.* 106:11594–9.
2. Harrison, O.J., X. Jin, S. Hong, F. Bahna, G. Ahlsen, J. Brasch, Y. Wu, J. Vendome, K. Felsovalyi, C.M. Hampton, R.B. Troyanovsky, A. Ben-Shaul, J. Frank, S.M. Troyanovsky, L. Shapiro, and B. Honig. 2011. The extracellular architecture of adherens junctions revealed by crystal structures of type I cadherins. *Structure.* 19:244–56.
3. Harrison, O.J., J. Brasch, G. Lasso, P.S. Katsamba, G. Ahlsen, B. Honig, and L. Shapiro. 2016. Structural basis of adhesive binding by desmocollins and desmogleins. *Proc. Natl. Acad. Sci. U. S. A.* 113:7160–5.
4. Dieding, M., J.D. Debus, R. Kerkhoff, A. Gaertner-Rommel, V. Walhorn, H. Milting, and D. Anselmetti. 2017. Arrhythmogenic cardiomyopathy related DSG2 mutations affect desmosomal cadherin binding kinetics. *Sci. Rep.* 7:13791.
5. Marcozzi, C., I.D. Burdett, R.S. Buxton, and A.I. Magee. 1998. Coexpression of both types of desmosomal cadherin and plakoglobin confers strong intercellular adhesion. *J. Cell Sci.*
6. Getsios, S., E. V. Amargo, R.L. Dusek, K. Ishii, L. Sheu, L.M. Godsel, and K.J. Green. 2004. Coordinated expression of desmoglein 1 and desmocollin 1 regulates intercellular adhesion. *Differentiation.* 72:419–433.
7. Waschke, J., P. Bruggeman, W. Baumgartner, D. Zillikens, and D. Drenckhahn. 2005. Pemphigus foliaceus IgG causes dissociation of desmoglein 1-containing junctions without blocking desmoglein 1 transinteraction. *J. Clin. Invest.* 115:3157–3165.
8. Rubinstein, R., C.A. Thu, K.M. Goodman, H.N. Wolcott, F. Bahna, S. Manne palli, G. Ahlsen, M. Chevee, A. Halim, H. Clausen, T. Maniatis, L. Shapiro, and B. Honig. 2015. Molecular Logic of Neuronal Self-Recognition through Protocadherin Domain Interactions. *Cell.* 163:629–42.
9. Goodman, K.M., R. Rubinstein, C.A. Thu, F. Bahna, S. Manne palli, G. Ahlsén, C. Rittenhouse, T. Maniatis, B. Honig, and L. Shapiro. 2016. Structural Basis of Diverse Homophilic Recognition by Clustered α - and β -Protocadherins. *Neuron.*
10. Goodman, K.M., R. Rubinstein, C.A. Thu, S. Manne palli, F. Bahna, G. Ahlsén, C. Rittenhouse, T. Maniatis, B. Honig, and L. Shapiro. 2016. γ -Protocadherin structural diversity and functional implications. *Elife.* 5.